

Molecular Physics

An International Journal at the Interface Between Chemistry and Physics

ISSN: (Print) (Online) Journal homepage: <https://www.tandfonline.com/loi/tmph20>

Electrostatic trapping vibrationally excited Rydberg NO molecules

M. H. Rayment & S. D. Hogan

To cite this article: M. H. Rayment & S. D. Hogan (2022): Electrostatic trapping vibrationally excited Rydberg NO molecules, Molecular Physics, DOI: [10.1080/00268976.2022.2160846](https://doi.org/10.1080/00268976.2022.2160846)

To link to this article: <https://doi.org/10.1080/00268976.2022.2160846>



© 2022 The Author(s). Published by Informa UK Limited, trading as Taylor & Francis Group.



Published online: 26 Dec 2022.



Submit your article to this journal [↗](#)



Article views: 86



View related articles [↗](#)



View Crossmark data [↗](#)

Electrostatic trapping vibrationally excited Rydberg NO molecules

M. H. Rayment  and S. D. Hogan 

Department of Physics and Astronomy, University College London, London, UK

ABSTRACT

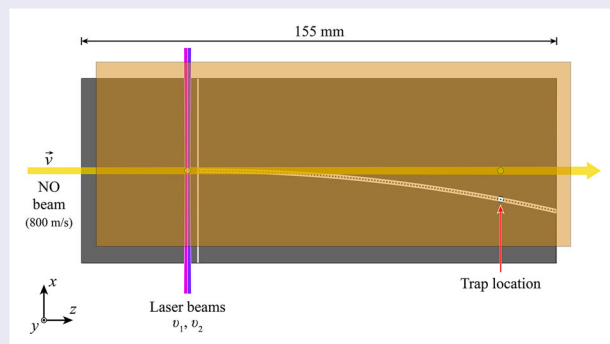
Nitric oxide (NO) molecules travelling in pulsed supersonic beams have been laser photoexcited to long-lived Rydberg states in series converging to the lowest lying, $v^+ = 0$, and first excited, $v^+ = 1$, vibrational states in the ground electronic state of NO^+ . After excitation, the molecules were decelerated in the travelling electric traps of a chip-based Rydberg–Stark decelerator. Deceleration to rest in the laboratory-fixed frame of reference allowed subsequent electrostatic trapping before *in situ* detection by pulsed electric field ionisation. The decay rates of the molecules from the traps were measured for states with principal quantum numbers between 32 and 48. Comparison of the corresponding trap decay time constants, ranging from 245 to 400 μs for states with $v^+ = 1$, with those recorded for molecules in states with $v^+ = 0$, allowed bounds to be placed on the vibrational autoionisation rates of the ℓ -mixed Stark states prepared in the experiments of < 60 Hz.

ARTICLE HISTORY

Received 18 September 2022
Accepted 16 December 2022

KEYWORDS

Rydberg states; cold molecules; electrostatic trapping; vibrational autoionisation





1. Introduction

Cold samples of gas-phase atoms and molecules in high Rydberg states, travelling in velocity-controlled beams or confined in traps, are of importance, for example, in studies of (1) excited state decay processes, including effects of blackbody radiation, spontaneous emission, dissociation and autoionisation [1–6]; (2) resonant energy transfer and van der Waals interactions [7–9]; and (3) ion-molecule reactions at low collision energies, or low translational temperatures [10–12]. These samples can be prepared in a general way, by exerting forces on excited molecules initially travelling in pulsed supersonic beams, using inhomogeneous electric fields [13–16]. This approach is referred to as Rydberg–Stark deceleration, and takes advantage of the large static electric dipole moments associated with ℓ -mixed Rydberg–Stark states

(ℓ is the orbital angular momentum quantum number of the Rydberg electron) [17]. These static electric dipole moments scale with n^2 , and exceed 3000 D for $n > 30$.

The implementation of scalable, chip-based Rydberg–Stark decelerators [18,19] has recently allowed deceleration to rest in the laboratory-fixed frame of reference, and electrostatic trapping of nitric oxide (NO) molecules [5]. In a 30 K cryogenic environment, molecules in Rydberg series converging to the lowest, $v^+ = 0$, vibrational state in the ground electronic state of NO^+ (v^+ is the vibrational quantum number of the NO^+ ion core), and principal quantum numbers, n , between 32 and 50 were trapped for times in excess of 1 ms. The time constants associated with the decay of the molecules from the traps ranged from 200 to 400 μs , and generally decreased as the value of n was increased. These

CONTACT S. D. Hogan  s.hogan@ucl.ac.uk  Department of Physics and Astronomy, University College London, Gower Street, London, WC1E 6BT UK

© 2022 The Author(s). Published by Informa UK Limited, trading as Taylor & Francis Group.
This is an Open Access article distributed under the terms of the Creative Commons Attribution License (<http://creativecommons.org/licenses/by/4.0/>), which permits unrestricted use, distribution, and reproduction in any medium, provided the original work is properly cited.

observations yielded new insights into effects of vibrational channel interactions on slow decay processes of long-lived molecular Rydberg states [6].

Here we report, deceleration and electrostatic trapping of vibrationally excited Rydberg molecules. In this case, the Rydberg states prepared by laser photoexcitation converged to the first excited, $\nu^+ = 1$, vibrational state in the $X^+1\Sigma^+$ ground electronic state of NO^+ . Since the particular states studied, with values of n between 32 and 48, and rotational quantum numbers $N^+ = 0, 1$, and 2, lie energetically above the lowest, $\nu^+ = 0$, ionisation limit of the molecule, they can, in addition to decaying by spontaneous emission and predissociation, also decay by autoionisation. Comparison of the measured decay rates of the molecules from the electrostatic traps with those recorded for molecules in states with $\nu^+ = 0$ has allowed bounds to be placed on the rates of vibrational autoionisation of the experimentally accessible long-lived Rydberg states. Together with their direct relevance to investigations of excited state decay dynamics, the decelerated and trapped Rydberg molecules prepared in the work described here are of interest for low-energy collision studies, including studies of resonant energy transfer and ion-molecule reactions, with a vibrationally excited ion core.

The remainder of this article is structured as follows: In Section 2 the apparatus and laser photoexcitation scheme used in the experiments are described. In Section 3, the results of measurements of quantum-state-dependent decay rates of electrostatically trapped molecules are presented, along with an analysis of the role of intramolecular interactions in the excited state decay dynamics. Finally, in Section 4 conclusions are drawn.

2. Experiment

2.1. Apparatus

The central part of the apparatus used in the experiments is depicted schematically in Figure 1. This setup is identical to that used in Refs. [5] and [6]. A pulsed valve, operated at a repetition rate of 25 Hz, was used to generate a supersonic beam of NO with a mean longitudinal speed of $\sim 810 \text{ ms}^{-1}$. After passing through a 2-mm-diameter skimmer the molecules entered into a region enclosed by a 30 K heat shield that contained the decelerator. Prior to deceleration and electrostatic trapping the molecules were photoexcited, between electrodes E1 and E2, to long-lived high- n ($n = 32$ to 48) Rydberg states using the $n\ell X^+1\Sigma^+ \leftarrow A^2\Sigma^+ \leftarrow X^2\Pi_{1/2}$ two-colour two-photon excitation scheme. This was driven by the counter-propagating frequency-tripled and frequency-doubled outputs of two Nd:YAG-pumped pulsed dye

lasers at wavenumbers ν_1 and ν_2 , respectively. Photoexcitation was implemented with ν_1 in two wavenumber ranges: $\nu_1 = 44,180 - 44,230 \text{ cm}^{-1}$ ($\equiv 226.3 - 226.1 \text{ nm}$), and $\nu_1 = 46,510 - 46,575 \text{ cm}^{-1}$ ($\equiv 215.0 - 214.7 \text{ nm}$) [$\sim 20 - 80 \mu\text{J}/\text{pulse}$], to access the $\nu' = 0$ and $\nu' = 1$ levels of the intermediate A state, respectively. In each case, ν_2 was adjusted in the wavenumber range from $30,420 \text{ cm}^{-1}$ to $30,500 \text{ cm}^{-1}$ ($\equiv 328.7$ to 327.8 nm) [$\sim 0.5 - 1.5 \text{ mJ}/\text{pulse}$] to excite high Rydberg states. For all experiments, a fibre-coupled wavelength meter was used to monitor and calibrate the vacuum wavelengths of the fundamental outputs of the dye lasers.

After photoexcitation, the molecules travelled for $\sim 5.4 \mu\text{s}$ (corresponding to a distance of $\sim 4 \text{ mm}$) in the z -dimension before being loaded into a single travelling electric trap of the decelerator. The travelling traps, for molecules in low-field-seeking (LFS) Rydberg–Stark states with positive Stark energy shifts, were generated by applying a set of 5 sinusoidally oscillating potentials of amplitude V_0 to the curved array of $0.5 \text{ mm} \times 0.5 \text{ mm}$ square electrodes in Figure 1. A potential of $-V_0/2$ was applied simultaneously to the flat metal electrode E2 located parallel to, and 3 mm above this array in the y dimension. The potential on the side electrodes (ground planes of the segmented transmission line that forms the decelerator) was set to zero for deceleration and trapping. Deceleration of the molecules was achieved by decelerating the travelling traps in which they were confined from 795 ms^{-1} to zero-mean-velocity in the laboratory-fixed frame of reference. This was implemented by chirping the frequency of the oscillating potentials from 160 to 0 kHz. The deceleration process took place over a distance of $\sim 100 \text{ mm}$, and in a time of $\sim 250 \mu\text{s}$.

Detection of the trapped molecules was performed by pulsed electric field ionisation (PFI) *in situ* at the position of the stationary electrostatic trap within the decelerator structure [20]. To implement this, the trapping potentials were switched off and a fast-rising potential of +500 V was applied to the side electrodes. NO^+ ions generated by ionisation of the Rydberg molecules in the resulting fields at the trap position, were then accelerated through the 2-mm-diameter aperture A1 in E2 and collected at a microchannel plate (MCP) detector. Rydberg state-selective electric field ionisation (SFI), could also be performed. This was carried out by applying a slowly-rising pulsed potential of the form $V_{\text{ramp}}(t) = -V_{\text{max}}[1 - \exp(-t/\tau_{\text{ramp}})]$, where $\tau_{\text{ramp}} = 4.4 \mu\text{s}$, to the side electrodes, with the ionised electrons collected at the same MCP detector. In this case, the short flight time of the electrons to the MCP ($\lesssim 10 \text{ ns}$) allowed the ionisation and detection times of the molecules to be correlated with $V_{\text{ramp}}(t)$ at the time of ionisation. To aid in the optimisation and alignment of the apparatus, PFI

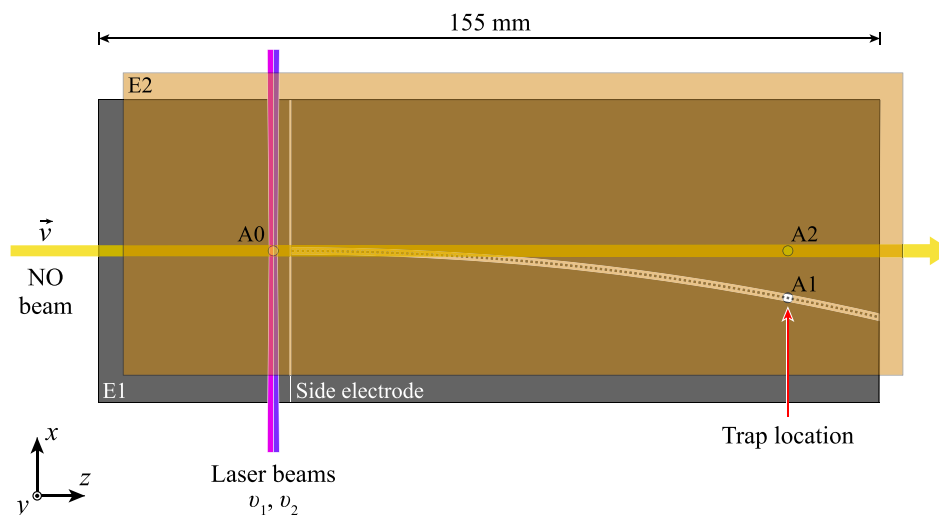


Figure 1. Schematic diagram of the chip-based Rydberg–Stark decelerator. The partially transparent electrode E2 is displaced vertically and to the right for clarity. Electrons and ions could be extracted through apertures A0, A1 and A2 in E2 and collected at MCP detectors following PFI. Note: Only one side electrode is labelled in the figure (see text for details).

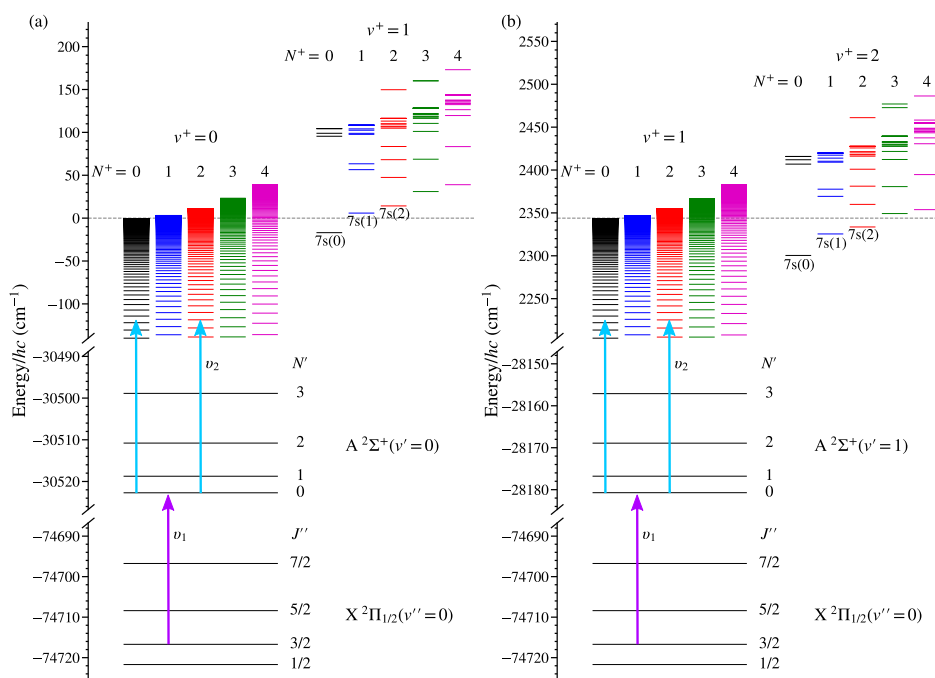


Figure 2. Resonance-enhanced two-colour two-photon excitation schemes used to prepare Rydberg states in NO converging to the (a) $v^+ = 0$, and (b) $v^+ = 1$ vibrational states in the $X^+ \Sigma^+$ ground electronic state of NO^+ . Low-lying $n = 7$ Rydberg states with $v^+ = 1$ and 2 are also included in each panel. All energies are displayed with respect to the energy of the $N^+ = 0, v^+ = 0$ Rydberg series limit.

could also be performed close to the laser photoexcitation region and on the molecular beam axis within the decelerator structure, with ion extraction through apertures A0 and A2, respectively.

2.2. Laser photoexcitation schemes

Rydberg states in NO were prepared using the $n\ell X^+ \Sigma^+(v^+, N^+) \leftarrow A^2 \Sigma^+(v', N', J') \leftarrow X^2 \Pi_{1/2}(v'', J'')$ resonance-enhanced two-colour two-photon excitation

schemes depicted in Figure 2 [21–29]. Laser radiation at wavenumber, ν_1 , was used to drive transitions between the $X^2 \Pi_{1/2}(v'' = 0)$ ground state and either the $A^2 \Sigma^+(v' = 0)$, or the $A^2 \Sigma^+(v' = 1)$ intermediate state. Spectra of these ground-to-intermediate state transitions were characterised by $(1+1')$ two-colour resonance-enhanced multi-photon ionisation (REMPI). By way of example, an $A(v' = 1) \leftarrow X(v'' = 0)$ $(1+1')$ REMPI spectrum is shown in Figure 3. When recording these data the value of ν_1 was varied while ν_2 was set to

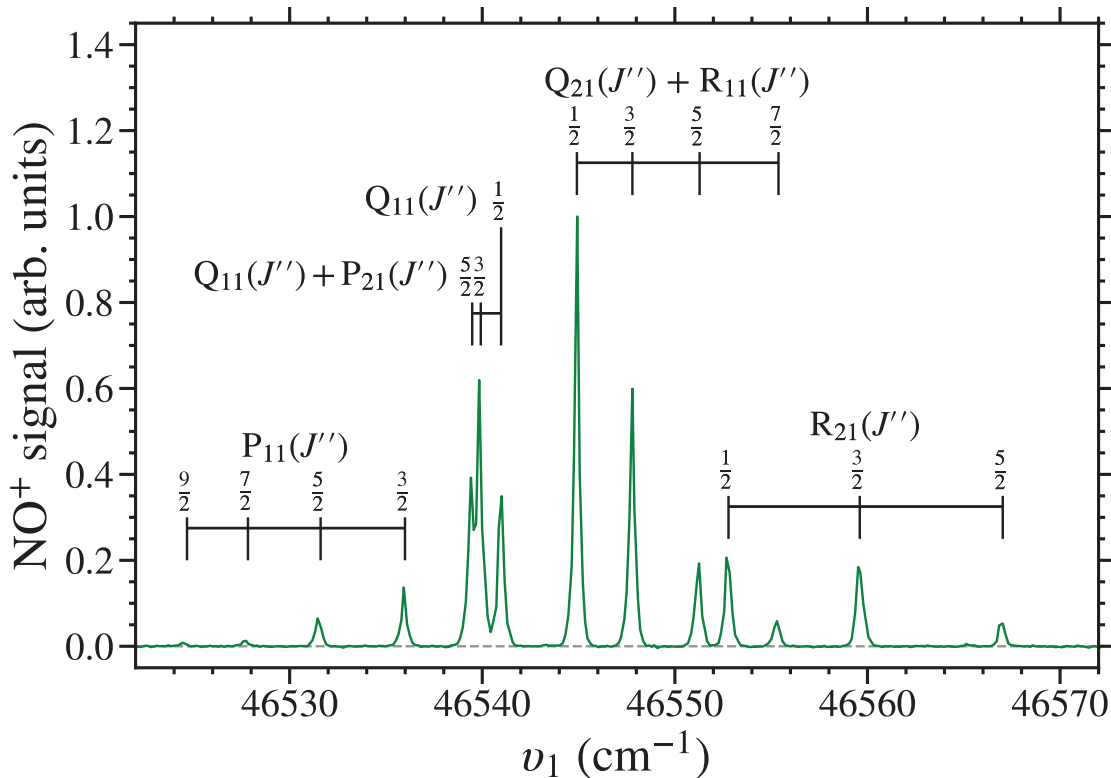


Figure 3. Two-colour (1+1') REMPI spectrum of the $A^2\Sigma^+(v' = 1) \leftarrow X^2\Pi_{1/2}(v'' = 0)$ transitions in NO.

30, 534.35 cm^{-1} (\equiv 327.500 nm) to photoionise excited molecules. The transitions in this spectrum are labelled using the $\Delta J_{f'f''}(J'')$ notation where J is the total angular momentum quantum number [26,30]. The labels P, Q, and R correspond to $\Delta J = -1, 0,$ and $+1$ transitions. The subscripts f' and f'' refer to the fine-structure of the of A and X states, respectively. All of the observed transitions are labelled with $f'' = 1$ because they originate from the lower, $X^2\Pi_{1/2}$, spin-orbit component of the ground state. In the A state, $f' = 1$ and 2 correspond to the states for which $J' = N' + 1/2$ and $N' - 1/2$, with the same value of N' . However, because the spin-orbit splitting in the A state is small, $\sim 0.005 \text{ cm}^{-1}$ [31,32], it was not resolved. The wavenumbers indicated by the labelled vertical bars in Figure 3 were calculated using the electronic, vibrational, and rotational constants for the X and A states listed in Table 1 [33,34]. A similar REMPI spectrum of the $A(v' = 0) \leftarrow X(v'' = 0)$ transitions was reported in Ref. [29]. From these measurements, the rotational temperature of the molecules in the supersonic beam was estimate to be $\sim 10 \text{ K}$.

The $A^2\Sigma^+$ state in NO is a low-lying Rydberg state. It, therefore, has a similar potential energy curve to the high- n Rydberg states, and the ground electronic state of NO^+ . Consequently, the Franck–Condon principle results in a propensity for $\Delta v = v^+ - v' = 0$ transitions from the intermediate A state to the high Rydberg states

Table 1. Electronic, vibrational, and rotational constants of the $X^2\Pi_{1/2}$ and $A^2\Sigma^+$ states in $^{14}\text{N}^{16}\text{O}$.

Quantity	$X^2\Pi_{1/2}$	$A^2\Sigma^+$
T_e	0	43,965.7
ω_e	1904.2	2374.31
$\omega_e X_e$	14.075	16.159
B_e	1.67195	1.9965
α_e	0.0171	0.01915
D_e	5.4×10^{-7}	5.4×10^{-6}

All quantities are expressed in cm^{-1} and were obtained from Refs. [33] and [34].

upon laser photoexcitation. Excitation to the $A^2\Sigma^+(v')$ state with $v' = 0$ or 1, therefore, allowed access to high Rydberg states converging to the $v^+ = 0$ or 1 states in the ground electronic state of NO^+ , respectively.

For all the measurements described here, v_1 was either set to 44,193.99 cm^{-1} (\equiv 226.275 nm), or 46,535.87 cm^{-1} (\equiv 214.888 nm) to populate the $v' = 0$, or $v' = 1$ vibrational states in the $A^2\Sigma^+(v', N' = 0, J' = 1/2)$ intermediate state on the $P_{11}(\frac{3}{2})$ resonance. In each case, the value of v_2 , was adjusted to excite optically accessible $n\ell(N^+) = np(0)$ and $nf(2)$ Rydberg states, with values of n in the range from 32 to 48. Long-lived ℓ -mixed Rydberg–Stark states were populated by ℓ - and M_N -mixing that occurred in weak time-varying electric fields close to the time of photoexcitation [29,35,36].

3. Results and discussion

3.1. Laser spectroscopy

To determine the range of values of n , and N^+ , of the Rydberg states in NO that could be decelerated and electrostatically trapped, laser photoexcitation spectra were recorded with selective detection of molecules that were successfully trapped. To achieve this, PFI was performed after a trapping time of $t_{\text{trap}} = 360 \mu\text{s}$ with the resulting spectra presented in Figure 4. All of the resonances in this figure correspond to the excitation of Rydberg states in series for which $\nu^+ = 1$ and represent resonances on which optically accessible $np(0)$ or $nf(2)$ character is mixed into near degenerate long-lived Rydberg–Stark states. Spectra recorded for $V_0 = 149$ and 100 V are displayed in Figure 4(b,c), respectively. The relative intensities of the features in these spectra reflect the combined effects of the efficiency with which long-lived LFS Rydberg–Stark states were populated at excitation, the deceleration and trap loading efficiency, and the lifetimes of the Rydberg states. Comparable spectra for Rydberg states with $\nu^+ = 0$ were reported in Ref. [6].

The transitions with maximal spectral intensity occur in Figure 4 for higher values of n when V_0 , the amplitude of the deceleration/trapping potentials, is reduced to 100 V . For a given value of V_0 , i.e., a particular depth of the electric field minima in the travelling electric traps, the optimal range of values of n for which deceleration and trapping can be achieved is determined by the Rydberg state electric dipole moments and ionisation electric fields. For lower values of n , the deceleration and trapping efficiency is reduced because of the n^2 dependence of the maximal static electric dipole moments of the Rydberg states, and therefore the maximal force that can exerted on the molecules. On the other hand, the n^{-4} dependence of the threshold ionisation electric field for high Rydberg states [29,37,38] results in a reduction in the deceleration and trapping efficiency for higher values of n . This is because, during the deceleration and trap loading process, molecules in higher n states are more likely to ionise, and the phase-space acceptance of the travelling electric traps for these states reduces. From numerical particle trajectory calculations, it was determined that the lower threshold for electric field ionisation of higher- n Rydberg states does not result in a significant increase in field ionisation after the traps are brought to rest.

Transitions to $nf(2)$ Rydberg states dominate the spectra in Figure 4 because of the comparatively small $n\ell$ quantum defects of ~ 0.02 in NO, and therefore the close proximity of these states to long-lived higher- ℓ $n(N^+) = n(2)$ states, where $n(N^+)$ refers to the ℓ -mixed hydrogenic Stark states. However, ℓ - and N^+ -mixing

involving optically accessible $np(0)$ states can also lead to the population of $[n-1](0)$ and $n'(1)$ Stark states. In these cases $[n-1](0)$ states are populated as a result of direct electric field-induced mixing with $np(0)$ states. $n'(1)$ Stark states, for which $n' \neq n$, are populated in situations where mixing with near degenerate $np(0)$ and $n'd(1)$ states occurs because of intramolecular charge-dipole interactions, combined with electric-field-induced mixing of $n'd(1)$ character into the $n'(1)$ states [39,40]. The measurements of trap decay rates reported here focus primarily on $n(2)$ Stark states excited on the $nf(2)$ resonances indicated by the horizontal bar across the top of Figure 4.

In addition to standard laser photoexcitation spectra, SFI of the Rydberg molecules was performed after deceleration and trapping for $t_{\text{trap}} = 100 \mu\text{s}$ with $V_0 = 149 \text{ V}$ [separated panels in Figure 4(a)]. This detection methodology allowed changes in the ionisation fields of the molecules in states with different values of n to be identified. These measurements were made by applying the slowly-rising potential, $V_{\text{ramp}}(t)$, in the right-hand panel of Figure 4(a) to the side electrodes after switching off the deceleration and trapping potentials. Normalised electron time-of-flight (TOF) distributions recorded by SFI following excitation on the resonances with values of n between 36 and 46 are displayed across the left part of Figure 4(a). The location of the maximum in each time-of-flight distribution, as determined by fitting an exponentially modified normal distribution, is denoted by a red marker. The widths of the distributions in the time domain reflect (1) the distribution of Rydberg–Stark states populated at the time of SFI, (2) the inhomogeneity of the ionisation fields within the decelerator structure, and (3) the motion of the molecules during SFI.

In general for the $nf(2)$ resonances, the maxima in the electron TOF distributions in Figure 4(a) occur at earlier times as the value of n increases. This reflects the n^{-4} scaling of the threshold ionisation electric field [41]. SFI measurements performed following excitation on the resonances at $\nu_2 = 30,462.50 \text{ cm}^{-1}$ and $30,463.24 \text{ cm}^{-1}$, i.e., the two resonances between the $38f(2)$ and $39f(2)$ features, aided in the characterisation of these states. The maxima in the electron TOF distributions in both of these cases occur at earlier times (4.5 and $4.9 \mu\text{s}$, respectively) than those associated with these $nf(2)$ resonances. Therefore the molecules excited on these resonances ionise in lower electric fields. This suggests excitation into states with values of $n > 39$. These states must therefore have values of $N^+ < 2$, and the higher wavenumber feature at $\nu_2 = 30,463.24 \text{ cm}^{-1}$ must have a lower value of n than the lower one. From the calculated energy-level structure of the Rydberg states, these resonances were attributed to

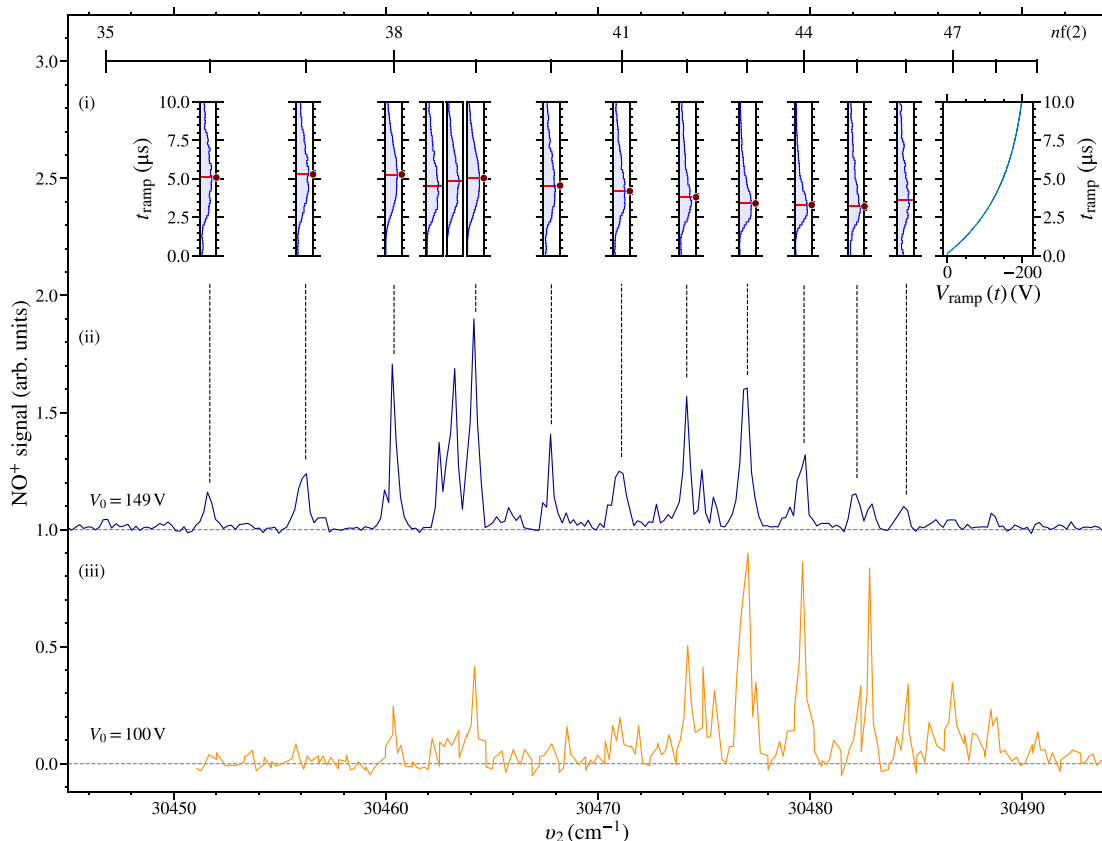


Figure 4. Spectra of long-lived $\nu^+ = 1$ Rydberg states in NO recorded by PFI after deceleration and electrostatic trapping for $t_{\text{trap}} = 360 \mu\text{s}$ with $\nu_1 = 46,535.87 \text{ cm}^{-1}$. When recording the data in spectrum (ii) the amplitude of the deceleration/trapping potentials was $V_0 = 149 \text{ V}$, and (iii) $V_0 = 100 \text{ V}$. The upper part (i) of the figure, contains electron time-of-flight distributions recorded by SFI with the ionisation potential $V_{\text{ramp}}(t)$ indicated on the top right. These data were recorded for $t_{\text{trap}} = 100 \mu\text{s}$, with $V_0 = 149 \text{ V}$ and excitation on the resonances indicated in (ii). The red horizontal line within each panel denotes the intensity maximum determined by fitting an exponentially modified normal distribution to each dataset.

the population of 42(0) and 41(1) Rydberg–Stark states, respectively.

3.2. Trap decay rates

Measurements of the decay of the electrostatically trapped Rydberg NO molecules were performed in a similar way to those described in Ref. [6]. After laser photoexcitation to Rydberg states with $\nu^+ = 0$ or 1, the molecules were decelerated and electrostatically trapped. The integrated NO^+ ion signal, recorded after PFI of the trapped molecules was then measured for values of t_{trap} up to 1 ms. Trap decay time constants, τ_{decay} , were then obtained by fitting single exponential functions to these data between $t_{\text{trap}} = 50$ and $350 \mu\text{s}$. The corresponding results are presented in Figure 5. Each data point in this figure corresponds to the weighted mean of up to 15 separate measurements of τ_{decay} . The error bars represent the uncertainties on these mean values.

In Figure 5, the measured values of τ_{decay} for $n(2)$ Rydberg states with $\nu^+ = 0$ (filled red circles – previously

presented in Ref. [6]) and $\nu^+ = 1$ (open blue diamonds), are shown for $n = 32–48$. All measurements were performed for $V_0 = 149 \text{ V}$. The general trend seen in these data is that as the value of n is increased, τ_{decay} decreases. This dependence is seen for the $n(2)$ states in both the $\nu^+ = 0$ and $\nu^+ = 1$ series and was previously observed for $n(0)$ and $n(1)$ states with $\nu^+ = 0$ [6]. The measured values of τ_{decay} , for states with $\nu^+ = 0$ and 1 agree within the measurement uncertainties. For example, in the case of the 38(2) states $\tau_{\text{decay}} = 346.2 \pm 3.4 \mu\text{s}$ when $\nu^+ = 0$, and $351.4 \pm 3.5 \mu\text{s}$ when $\nu^+ = 1$. For individual states in both series, deviations from the general trend are observed. These occur, for example, on the 43(2) resonance where the measured values of τ_{decay} are larger than expected from the surrounding states.

The trap decay times, τ_{decay} , in Figure 5, do not follow the $\sim n^4$ -scaling expected for the lifetimes of ℓ -mixed Rydberg–Stark states in atoms [41]. The general trend in the measured values of τ_{decay} , and the deviations from this trend result from weak intramolecular interactions [6]. Because of the carefully controlled experimental

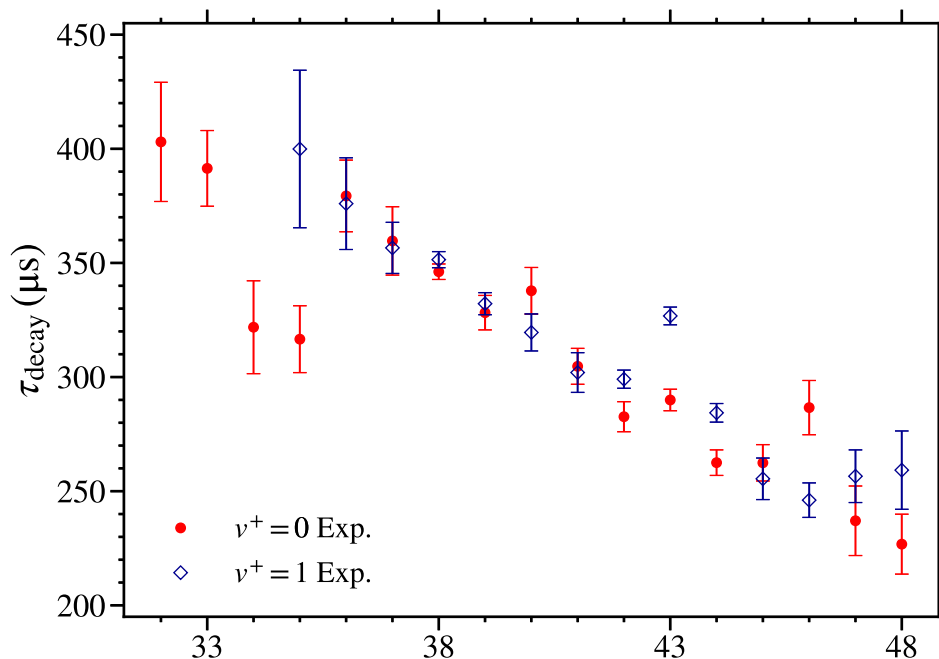


Figure 5. Measured trap decay time constants, τ_{decay} , for $n(2)$ Rydberg states converging to the $\nu^+ = 0$ (filled red circles – previously reported in Ref. [6]), and $\nu^+ = 1$ (open blue diamonds) states in the ground electronic state of NO^+ . For all measurements $V_0 = 149$ V.

conditions, contributions from collisions (the number density of the trapped molecules is $\sim 10^5 \text{ cm}^{-3}$) and blackbody-induced transitions (the trap environment is maintained at ~ 30 K) can be ruled out as playing a significant role. To investigate the effect of electric field ionisation on the decay of trapped molecules, numerical particle trajectory calculations, that included a Monte-Carlo treatment of the electric field ionisation process, were performed. These indicated that electric field ionisation contributes < 1 Hz to the decay rate from the traps for the values of n studied here.

The general decrease in the values of τ_{decay} with increasing n arises because of weak vibrational channel interactions. These interactions occur between $\nu^+ = 0$ ($\nu^+ = 1$) high- n Rydberg states, and short-lived $n = 7$ states with $\nu^+ = 1$ ($\nu^+ = 2$). As seen in Figure 2, the $n = 7$ states with $\nu^+ = 1$ ($\nu^+ = 2$) lie energetically above, but close to, the $N^+ = 0$, $\nu^+ = 0$ ($\nu^+ = 1$) Rydberg series limit. Previous spectroscopic studies of low- n Rydberg states in NO with $\nu^+ = 1$ concluded that their lifetimes are dominated by fast non-radiative decay, and that the $n = 7$, $\nu^+ = 1$ states in particular have lifetimes of ~ 1 ps [25,27]. Consequently, a contribution of 1 part in 10^9 of $n = 7$, $\nu^+ = 1$ character admixed into the $\nu^+ = 0$ Rydberg–Stark states increases their decay rate by ~ 1 kHz. This amount of mixing is consistent with that expected from a simple two-state quantum-mechanical model. It is also comparable to the calculated fluorescence decay rates of these long-lived Rydberg states [6].

In the data in Figure 5, the values of τ_{decay} for the $n(2)$ Rydberg states with $\nu^+ = 0$ and 1 are similar, and in both cases decrease as n increases. This leads to the conclusion that a comparable amount of mixing occurs between the $n(2)$ states with $\nu^+ = 1$ and the $n = 7$, $\nu^+ = 2$ states, to that encountered for the $\nu^+ = 0$ Rydberg states. As seen in Figure 2, the $n = 7$, $\nu^+ = 1$ and 2 states lie in similar energetic positions with respect to the $n(2)$, $\nu^+ = 0$ and 1 states, respectively, which is consistent with similar contributions from vibrational channel interactions in both cases.

For several of the $n(2)$ resonances in Figure 5, deviations from the general trend exhibited by the data are seen for states with $\nu^+ = 0$ and 1. In each of these cases, because of accidental near degeneracies, Rydberg–Stark states with more than one set of values of n and N^+ are simultaneously populated upon photoexcitation, decelerated and trapped. For the $\nu^+ = 0$ states, these near degeneracies are discussed in Ref. [6]. For $\nu^+ = 1$, the main deviation from the general trend is seen on the 43(2) resonance. In this instance, molecules in 43(2) and 48(0) Rydberg–Stark states are simultaneously confined in the trap following photoexcitation on the 43f(2) resonance. The 43(2) Rydberg–Stark states are populated because of electric-field-induced mixing with the optically accessible 43f(2) states. Charge-quadrupole interactions, that couple states for which $\Delta N^+ = \pm 2$ and $\Delta \ell = 0$, also mix 43f(2) character into the near degenerate 48f(0) state, which, in the presence of weak stray electric fields mix further with the 48(0) Stark states. Since the 48(0) Stark

states decay more slowly from the trap than the 43(2) states – because of their lower value of N^+ and higher value of n – simultaneously trapping molecules in both states results in a value of τ_{decay} that is longer than for surrounding states in the $n(2)$ series.

3.3. Deceleration and trapping field strengths

The dependence of τ_{decay} on the strength of the trapping fields was investigated by comparing measurements for $n(2)$ states with $\nu^+ = 1$ made with $V_0 = 149$ V [open blue diamonds] and 100 V [filled orange squares] as presented in Figure 6. No measurement of τ_{decay} was made for the 40(2) state with $V_0 = 100$ V because the signal was insufficient. In general, for both values of V_0 , τ_{decay} decreases with increasing n . However, the values of τ_{decay} for $V_0 = 100$ V are in many instances greater than those for $V_0 = 149$ V. Although, for excitation on the 38(2) and 39(2) resonances the opposite behaviour is seen.

The measurements in Figure 6 demonstrate the persistence of the vibrational channel interactions that cause the general reduction in the measured values of τ_{decay} with increasing n at lower trap depths. The slight increase in τ_{decay} for values of n between 41 and 48 when $V_0 = 100$ V, compared to that for $V_0 = 149$ V, reflects the lower time-averaged field strength experienced by the trapped molecules. This lower field results in reduced Stark shifts, by a factor of $\sim 2/3$, of the trapped molecules. Since the Stark shifts of the LFS Stark states suitable for trapping are positive, reducing them leads to an increase in the average energy separation from the short-lived $n = 7$ states with $\nu^+ = 2$ which do not shift appreciably in the trapping fields. As a result, the amount of mixing with these states that occurred is slightly reduced and the trap decay times are longer.

The deviation of the value of τ_{decay} for the 43(2) resonance in Figure 6, from the general trend exhibited by the surrounding states, is more pronounced when $V_0 = 100$ V than when $V_0 = 149$ V. This is because the difference in the deceleration and trapping efficiency for the 43(2) and 48(0) Stark states excited on this resonance is more pronounced for lower values of V_0 . Consequently, the fraction of trapped molecules in the longer-lived 48(0) states is greater under these conditions and τ_{decay} increases.

Finally, the values of τ_{decay} decrease on the 38(2) and 39(2) resonances when V_0 is reduced to 100 V. This is attributed to a change in the distribution of Stark states populated in the trap. For lower trap potentials, states with smaller dipole moments are trapped less efficiently than those with larger dipole moments. Therefore, for a given value of n , a smaller range of Stark states will be efficiently trapped when $V_0 = 100$ V, than when $V_0 =$

149 V. The changes in these measured values of τ_{decay} reflect differences in the lifetimes of individual components within a manifold of ℓ -mixed Rydberg–Stark states, and in particular the fact that the outermost Stark states with the largest static electric dipole moments generally exhibit the shortest of these lifetimes.

3.4. Vibrational autoionisation

Because the Rydberg–Stark states with $\nu^+ = 1$ lie above the $\nu^+ = 0$ series limit, they can decay by vibrational autoionisation. Spontaneous emission from these states, and predissociation are expected to contribute in a similar way to the total decay rates of $n(2)$ Stark states with both $\nu^+ = 0$ and 1. Therefore, a comparison of the values of τ_{decay} for states in these two Rydberg series allows the effects of vibrational autoionisation on the decay of the long-lived $\nu^+ = 1$ Rydberg–Stark states in the trap to be inferred. Because the values of τ_{decay} for the $\nu^+ = 0$ and 1 states agree to within the experimental uncertainties, it is concluded that vibrational autoionisation does not play a significant role in the decay of the trapped molecules when $\nu^+ = 1$. An upper bound on the rate of vibrational autoionisation of these states, $\gamma_{\text{vib-trap}}$, can be obtained by considering the contribution required for τ_{decay} to change by twice the measurement uncertainty. This suggests that for $n = 38$, $\gamma_{\text{vib-trap}} \lesssim 60$ Hz.

Studies reported previously of the decay dynamics of Rydberg states in NO with values of $\ell \leq 4$, included detailed analyses of the effects of vibrational autoionisation [25,27,42–44]. In these works, it was shown that these low- ℓ Rydberg states with $\nu^+ = 0$ and 1 decay predominantly by fast non-radiative processes. However, in contrast to the $\nu^+ = 0$ states, for which predissociation is the dominant decay pathway, the $\nu^+ = 1$ Rydberg states predissociate and autoionise. Recent measurements of the decay rates of $ng(N^+)$ Rydberg states with $\nu^+ = 1$ and $n = 22, 25$, and 28, yielded total decay rates proportional to n^{-3} ($\sim 4 \times 10^{11} n^{-3}$ Hz averaged over all rotations and sub-states, i.e. ~ 20 MHz at $n = 28$) [44]. Calculations of the autoionisation rates, using a long-range potential model [44,45], indicated that $\sim 70\%$ of the total decay rate of these states could be attributed to autoionisation, with the remaining $\sim 30\%$ associated with predissociation. This is in line with previously measured predissociation rates of $ng(N^+)$ states with $\nu^+ = 0$ [42]. For all of the short-lived states studied in these works, the spontaneous emission rates were approximately three orders of magnitude lower than the autoionisation rates.

To connect these previous results to the measurements reported here for long-lived, ℓ -mixed Rydberg–Stark states, the vibrational autoionisation rates predicted by the long-range potential model were extrapolated to

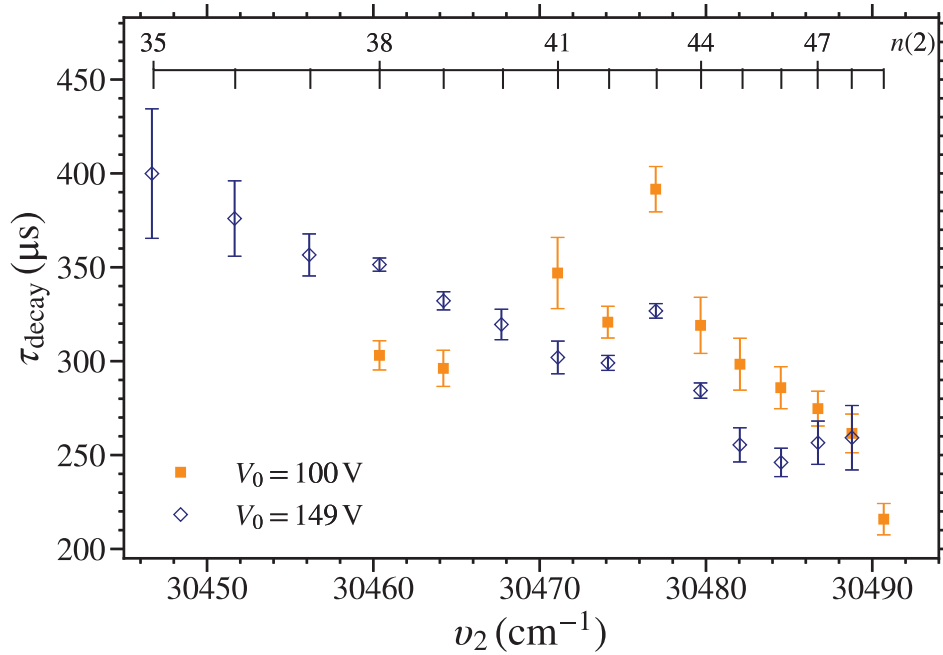


Figure 6. Measured trap decay time constants, τ_{decay} , for $n(2)$ Rydberg states with $v^+ = 1$. The data were recorded for $V_0 = 149$ V (open blue diamonds), and $V_0 = 100$ V (filled orange squares).

higher values of ℓ [44,45]. This allowed a rough estimate of the order of magnitude of the n - and ℓ -dependent vibrational autoionisation rates, $\gamma_{\text{vib}}(n, \ell)$, given by

$$\gamma_{\text{vib}}(n, \ell) \simeq 10^{16} n^{-3} \ell^{-8} \text{ Hz.} \quad (1)$$

From this expression, it is determined that the vibrational autoionisation rates of $n = 38$ Rydberg states with values of ℓ between 4 and 12 may be expected to lie between $\gamma_{\text{vib}}(38, 4) \sim 1$ MHz and $\gamma_{\text{vib}}(38, 12) \sim 100$ Hz. The spontaneous emission rates of these same states are between 10 and 1 kHz.

The molecules that were successfully decelerated and trapped in the experiments reported here were those in outer LFS Rydberg–Stark states. Calculations of the vibrational autoionisation rates of these states, for $n = 38$ and $M_N = 4$, and in Stark manifolds with $\ell_{\text{min}} = 4, 5$, and 6 (in an atom these would correspond to $m_\ell = 4, 5$, and 6 manifolds, respectively) were therefore made to aid in the interpretation of the experimental data. In these calculations, the vibrational autoionisation rate of a Stark state $|i\rangle$ was determined by decomposing it into Hund’s-case-(d) basis states $|k\rangle = |n_k \ell_k N_k^+ N_k M_{Nk}\rangle$, such that

$$\gamma_{\text{vib-calc},i} = \sum_k |c_{ik}(F_z)|^2 \gamma_{\text{vib}}(n_k, \ell_k), \quad (2)$$

where $c_{ik}(F_z) = \langle k|i(F_z)\rangle$ are the coefficients of the corresponding eigenvector in the electric field, F_z . These coefficients were calculated by the matrix diagonalisation methods described in Ref. [6]. The typical time-averaged

electric field strength of $\bar{F}_z = 95 \text{ V cm}^{-1}$, experienced by the molecules as they moved within the traps was determined through numerical particle trajectory calculations, and used in the calculations. By accounting for the n - and ℓ -dependence of $\gamma_{\text{vib}}(n, \ell)$ using the expression in Equation (1), the vibrational autoionisation rates obtained for the outermost LFS Stark states with $\ell_{\text{min}} = 4, 5$, and 6 were ~ 3 , ~ 0.7 , and ~ 0.2 kHz, respectively. These rates are all an order of magnitude, or more, larger than the experimentally determined bound of $\gamma_{\text{vib-trap}} \lesssim 60$ Hz.

To obtain further insight into the link between the experimental data and these crude order of magnitude estimates, the vibrational autoionisation rates of the field-free $|n\ell\rangle$ Rydberg states were considered more generally to have the form

$$\gamma_{\text{vib}}(n, \ell) = A n^{-3} \ell^{-p}, \quad (3)$$

where A and p are adjustable parameters. To explore the range of values of A and p that could result in Rydberg–Stark state vibrational autoionisation rates $\lesssim 60$ Hz, these parameters were constrained to ensure that $\gamma_{\text{vib}}(n, 4)$ was equal to the values reported recently for Rydberg states with $N^+ = 2$ in Ref. [44]. This was achieved by adjusting the value of A for each value of p . For these tests the value of p was chosen to lie between 6 and 18 because the intramolecular charge-dipole, charge-quadrupole, and charge-induced-dipole interactions scale with $\ell^{-5} - \ell^{-7}$, $\ell^{-3} - \ell^{-9}$, and $\ell^{-5} - \ell^{-7}$, respectively [40]. And, considering Fermi’s Golden

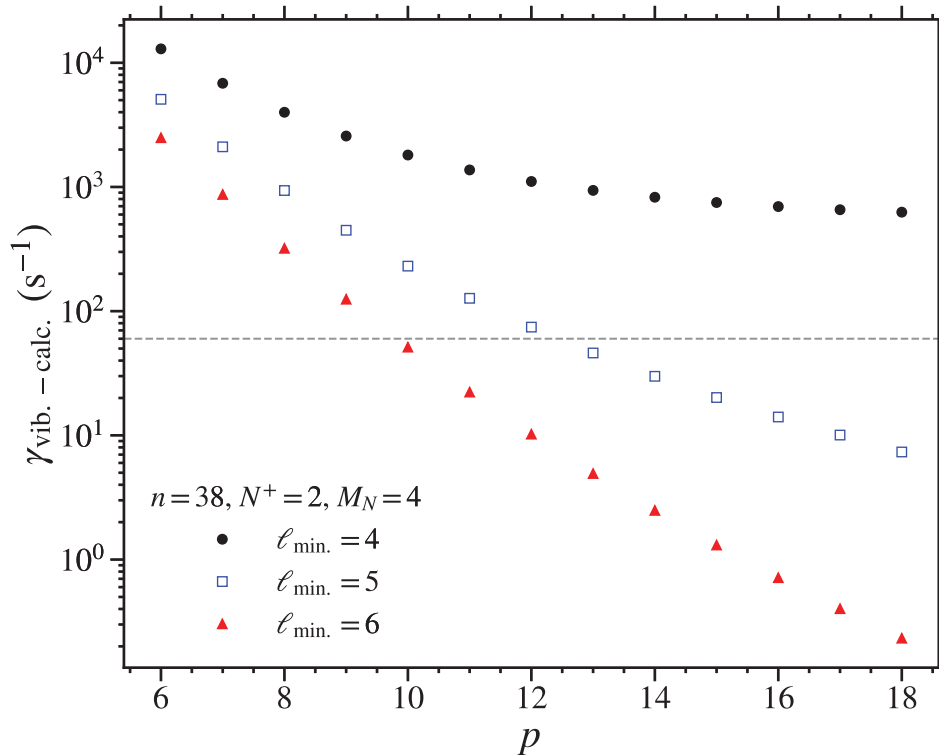


Figure 7. Calculated vibrational autoionisation rates of the outermost LFS Stark states with $n = 38$ and $M_N = 4$ in manifolds for which the minimum ℓ character considered was $\ell_{\text{min}} = 4$ (black circles), 5 (open blue squares), and 6 (red triangles) (see text for details).

Rule, the corresponding vibrational autoionisation rates would depend on the square of these quantities.

The calculated values of $\gamma_{\text{vib.} - \text{calc}}$ for the outermost LFS Stark states with $n = 38$ and $M_N = 4$ in manifolds with $\ell_{\text{min}} = 4, 5$, and 6 are shown in Figure 7. From these data, it is seen that when $\ell_{\text{min}} = 4$, $\gamma_{\text{vib.} - \text{calc}}$ converges to ~ 600 Hz as the value of p is increased. This represents the field-free $\ell = 4$ vibrational autoionisation rate for this value of n . Because the experimental bound on the vibrational autoionisation rates in the work reported here (dashed horizontal line) lies below $\gamma_{\text{vib.} - \text{calc}}$ for all values of p under these conditions, it is concluded that the Rydberg states of the decelerated and trapped molecules cannot possess any $\ell \leq 4$ character. For $\ell_{\text{min}} = 5$ and 6, the calculated vibrational autoionisation rates do reduce below 60 Hz for $p \gtrsim 12$, and 10, respectively. In both of these cases, the fluorescence rates of the field-free Rydberg states exceed the vibrational autoionisation rates for $\ell \gtrsim 8$. The ℓ -scaling suggested by these observations is stronger than that in Equation (1). However, because even crude estimates of the kind outlined here of vibrational autoionisation rates of ℓ -mixed Rydberg–Stark states are very sensitive to the vibrational autoionisation rates of the field-free low- ℓ states, a more precise interpretation of the experimental results will require more accurate values of the vibrational autoionisation rates of the field-free Rydberg states with $\ell > 4$.

4. Conclusions

The experiments reported here represent the first in which Rydberg molecules have been decelerated and electrostatically trapped in vibrationally excited states. The measured trap decay time constants exhibit a similar general reduction as the value of n is increased, to those for $\nu^+ = 0$ Rydberg–Stark states studied previously. This behaviour is attributed to the effects of vibrational channel interactions that couple long-lived high- n Rydberg states with a given value of ν^+ , to short-lived $n = 7$ states with $\nu^{+'} = \nu^+ + 1$. Comparison of the decay rates of the trapped vibrationally excited Rydberg molecules, with those for samples in states converging to the ground vibrational state of the NO^+ ion core, has allowed bounds to be placed on the rates of vibrational autoionisation of the ℓ -mixed Rydberg–Stark states. A crude numerical analysis based on extrapolation of vibrational autoionisation rates of low- ℓ Rydberg states to the states of interest here with higher values of ℓ , leads to the conclusion that the minimum- ℓ character of the Stark states of the trapped molecules must be ≥ 5 . Therefore, the minimum value of $|M_N|$ must at least fulfil the condition that $|M_N| > |N^+ - 4|$. A more detailed interpretation of these results will benefit from experiments performed with molecules decelerated and trapped in individual Rydberg–Stark states with selected values of $|M_N|$. This could be achieved by combining high-resolution laser

photoexcitation with population transfer between Stark states driven by microwave or millimetre-wave radiation. A more complete theoretical treatment of the Stark effect in the Rydberg states of NO that combines, for example, multichannel quantum defect theory with input from experiments and the results of quantum chemical calculations to allow links to be made between channel interactions and the interactions of the Rydberg electron with the multipole moments of the ion core, will also be of great value.

Acknowledgments

We are grateful to Prof R. W. Field (MIT) and Prof T. Barnum (Union College, New York) for valuable discussions relating to vibrational autoionisation of Rydberg states in NO.

Disclosure statement

No potential conflict of interest was reported by the author(s).

Funding

This work was supported by the European Research Council (ERC) under the European Union's Horizon 2020 research and innovation program [grant number 683341]. MHR is grateful to the Engineering and Physical Sciences Research Council (EPSRC) for support through their Doctoral Training Partnership [grant number EP/R513143/1].

ORCID

M. H. Rayment  <http://orcid.org/0000-0002-1532-0264>

S. D. Hogan  <http://orcid.org/0000-0002-7720-3979>

References

- [1] C. Seiler, S.D. Hogan, H. Schmutz, J.A. Agner and F. Merkt, *Phys. Rev. Lett.* **106**, 073003 (2011). doi:10.1103/PhysRevLett.106.073003
- [2] C. Seiler, Ph. D. thesis, ETH Zurich, 2013.
- [3] C. Seiler, J.A. Agner, P. Pillet and F. Merkt, *Mol. Opt. Phys.* **49**, 094006 (2016). doi:10.1088/0953-4075/49/9/094006
- [4] V. Zhelyazkova, M. Žeško, H. Schmutz, J.A. Agner and F. Merkt, *Mol. Phys.* **117**, 2980 (2019). doi:10.1080/00268976.2019.1600060
- [5] A. Deller, M.H. Rayment and S.D. Hogan, *Phys. Rev. Lett.* **125**, 73201 (2020). doi:10.1103/PhysRevLett.125.073201
- [6] M.H. Rayment and S.D. Hogan, *Phys. Chem. Chem. Phys.* **23**, 18806 (2021). doi:10.1039/D1CP01930A
- [7] V. Zhelyazkova and S.D. Hogan, *Phys. Rev. A* **95**, 042710 (2017). doi:10.1103/PhysRevA.95.042710
- [8] F. Jarisch and M. Zeppenfeld, *N. J. Phys.* **20**, 113044 (2018). doi:10.1088/1367-2630/aaf02e
- [9] K. Gawlas and S.D. Hogan, *J. Phys. Chem. Lett.* **11**, 83 (2020). doi:10.1021/acs.jpcclett.9b03290
- [10] P. Allmendinger, J. Deiglmayr, K. Höveler, O. Schullian and F. Merkt, *J. Chem. Phys.* **145**, 244316 (2016). doi:10.1063/1.4972130
- [11] V. Zhelyazkova, F.B.V. Martins, J.A. Agner, H. Schmutz and F. Merkt, *Phys. Rev. Lett.* **125**, 263401 (2020). doi:10.1103/PhysRevLett.125.263401
- [12] F. Merkt, K. Höveler and J. Deiglmayr, *J. Phys. Chem. Lett.* **13**, 864 (2022). doi:10.1021/acs.jpcclett.1c03374
- [13] W.H. Wing, *Phys. Rev. Lett.* **45**, 631 (1980). doi:10.1103/PhysRevLett.45.631
- [14] T. Breeden and H. Metcalf, *Phys. Rev. Lett.* **47**, 1726 (1981). doi:10.1103/PhysRevLett.47.1726
- [15] E. Vliegen, H.J. Wörner, T.P. Softley and F. Merkt, *Phys. Rev. Lett.* **92**, 033005 (2004). doi:10.1103/PhysRevLett.92.033005
- [16] Y. Yamakita, S.R. Procter, A.L. Goodgame, T.P. Softley and F. Merkt, *J. Chem. Phys.* **121**, 1419 (2004). doi:10.1063/1.1763146
- [17] S.D. Hogan, *EPJ Techn. Instrum.* **3**, (2016). doi:10.1140/epjti/s40485-015-0028-4
- [18] S.D. Hogan, P. Allmendinger, H. Saßmannshausen, H. Schmutz and F. Merkt, *Phys. Rev. Lett.* **108**, 063008 (2012). doi:10.1103/PhysRevLett.108.063008
- [19] P. Lancuba and S.D. Hogan, *Phys. Rev. A* **90**, 053420 (2014). doi:10.1103/PhysRevA.90.053420
- [20] P. Lancuba and S.D. Hogan, *Mol. Opt. Phys.* **49**, 074006 (2016). doi:10.1088/0953-4075/49/7/074006
- [21] T. Ebata, Y. Anezaki, M. Fujii, N. Mikami and M. Ito, *J. Phys. Chem.* **87**, 4773 (1983). doi:10.1021/j150642a001
- [22] M. Seaver, W.A. Chupka, S.D. Colson and D. Gauyacq, *J. Phys. Chem.* **87**, 2226 (1983). doi:10.1021/j100235a036
- [23] D.T. Biernacki, S.D. Colson and E.E. Eyler, *J. Chem. Phys.* **88**, 2099 (1988). doi:10.1063/1.454091
- [24] D.T. Biernacki, S.D. Colson and E.E. Eyler, *J. Chem. Phys.* **89**, 2599 (1988). doi:10.1063/1.455008
- [25] A. Fujii and N. Morita, *J. Chem. Phys.* **97**, 327 (1992). doi:10.1063/1.463631
- [26] E.F. McCormack, F. Di Teodoro, J.M. Grochocinski and S.T. Pratt, *J. Chem. Phys.* **109**, 63 (1998). doi:10.1063/1.476540
- [27] A.L. Goodgame, H. Dickinson, S.R. Mackenzie and T.P. Softley, *J. Chem. Phys.* **116**, 4922 (2002). doi:10.1063/1.1450552
- [28] R. Patel, N.J. Jones and H.H. Fielding, *J. Phys. B* **40**, 1369 (2007). doi:10.1088/0953-4075/40/7/006
- [29] A. Deller and S.D. Hogan, *J. Chem. Phys.* **152**, 144305 (2020). doi:10.1063/5.0003092
- [30] J.M. Brown, J.T. Hougen, K.P. Huber, J.W. Johns, I. Kopp, H. Lefebvre-Brion, A.J. Merer, D.A. Ramsay, J. Ros-tas and R.N. Zare, *J. Mol. Spectrosc.* **55**, 500 (1975). doi:10.1016/0022-2852(75)90291-X
- [31] T. Bergeman and R.N. Zare, *J. Chem. Phys.* **61**, 4500 (1974). doi:10.1063/1.1681767
- [32] J.A. Gray, R.L. Farrow, J.L. Durant and L.R. Thorne, *J. Chem. Phys.* **99**, 4327 (1993). doi:10.1063/1.466086
- [33] K.P. Huber and G. Herzberg, *Molecular Spectra and Molecular Structure: IV. Constants of Diatomic Molecules* (Springer, Boston (MA), 1979).
- [34] M. Sharma, J.M. Austin, N.G. Glumac and L. Massa, *AIAA J.* **48**, 1434 (2010). doi:10.2514/1.J050047
- [35] W.A. Chupka, *J. Chem. Phys.* **98**, 4520 (1993). doi:10.1063/1.465011
- [36] F. Merkt and R.N. Zare, *J. Chem. Phys.* **101**, 3495 (1994). doi:10.1063/1.467534
- [37] M.G. Littman, M.M. Kash and D. Kleppner, *Phys. Rev. Lett.* **41**, 103 (1978). doi:10.1103/PhysRevLett.41.103

- [38] R.J. Damburg and V.V. Kolosov, *J. Phys. B* **12**, 2637 (1979). doi:[10.1088/0022-3700/12/16/011](https://doi.org/10.1088/0022-3700/12/16/011)
- [39] M. Bixon and J. Jortner, *J. Chem. Phys.* **105**, 1363 (1996). doi:[10.1063/1.472033](https://doi.org/10.1063/1.472033)
- [40] M. Bixon and J. Jortner, *Mol. Phys.* **89**, 373 (1996). doi:[10.1080/002689796173787](https://doi.org/10.1080/002689796173787)
- [41] T.F. Gallagher, *Rydberg Atoms* (Cambridge University Press, Cambridge (UK), 1994).
- [42] A. Fujii and N. Morita, *J. Chem. Phys.* **103**, 6029 (1995). doi:[10.1063/1.470431](https://doi.org/10.1063/1.470431)
- [43] R.S. Minns, D.T. Lazenby, F.H. Hall, N.J. Jones, R. Patel and H.H. Fielding, *Mol. Phys.* **112**, 1808 (2014). doi:[10.1080/00268976.2013.865809](https://doi.org/10.1080/00268976.2013.865809)
- [44] T.J. Barnum, G. Clausen, J. Jiang, S.L. Coy and R.W. Field, *J. Chem. Phys.* **155**, 244303 (2021). doi:[10.1063/5.0070879](https://doi.org/10.1063/5.0070879)
- [45] E.E. Eyler, *Phys. Rev. A* **34**, 2881 (1986). doi:[10.1103/PhysRevA.34.2881](https://doi.org/10.1103/PhysRevA.34.2881)